Mid-wavelength Infrared Avalanche Photodetector with AlAsSb/GaSb Superlattice

Jiakai Li
Northwestern University
Arash Dehzangi
Northwestern University
Gail Brown
Northwestern University
Manijeh Razeghi (razeghi@northwestern.edu)
Northwestern University

Research Article

Keywords: mid-wavelength infrared, SAM-APD, AlGaAsSb/GaSb, InAsSb

Posted Date: January 6th, 2021

DOI: https://doi.org/10.21203/rs.3.rs-137300/v1

Version of Record: A version of this preprint was published at Scientific Reports on March 29th, 2021. See the published version at https://doi.org/10.1038/s41598-021-86566-8.

Mid-wavelength infrared avalanche photodetector with AlAsSb/GaSb superlattice

Jiakai Li, Arash Dehzangi, Gail Brown, Manijeh Razeghi[1*]

[1]Center for Quantum Devices, Department of Electrical Engineering and Computer Science, Northwestern University, Evanston, Illinois 60208

**Corresponding author: razeghi@eecs.northwestern.edu*

Abstract

This work demonstrates a mid-wavelength infrared separate absorption and multiplication avalanche photodiode (SAM-APD) with AlGaAsSb/GaSb multi-quantum well as the multiplication layer and InAsSb bulk material as the absorption layer. The InAsSb-based SAM-APD structure was grown by molecular beam epitaxy. The device exhibits a 100 % cut-off wavelength of ~5.3 µm at 150 K and ~5.6 µm at 200 K. At 150 K and 200 K, the responsivity of the SAM-APD reaches a peak value of 2.26 A/W and 3.84 A/W at 4.0 µm under -1.0 V applied bias, respectively. The SAM-APD device was designed to have electron dominated avalanching mechanism via the multi-quantum well structure as the avalanche architecture. A multiplication gain value of 29 at 200 K was achieved under −14.7 V bias voltage. The electron and hole impact ionization coefficients were calculated and compared. A carrier ionization ratio of ~0.097 was achieved at 200 K.

Mid-wavelength infrared (MWIR) photodetectors which can operate under the low flux conditions are of great interest for long-range military and astronomical applications.[1, 2] In most of these applications there is a need to increase the capability of the system to detect light in a low photon flux situation. Therefore, gain-based devices such as heterojunction phototransistors (HPTs) and avalanche photodiodes (APDs) are used to achieve the necessary photoresponse when the incoming photon flux is low.[3-5] Compared with the HPTs, the APDs can amplify weak signals without the relatively more complicated HPT device structure.[6]

For MWIR APD devices, HgCdTe is the state-of-art material system and has been widely used in infrared APDs.[7, 8] However, the HgCdTe-based APDs suffer from drawbacks such as material instability and low fabrication yields. [9, 10] The emerging material system, antimony-based strained layer superlattices (SLS) have drawn lots of attention due to the advantages of high material uniformity, great bandgap tunability and Auger recombination suppression compared with HgCdTe detectors.[11-14] Recently, the MWIR APDs based on III-V superlattices have been demonstrated.[15] However, their performance, especially the excess noise factor, is limited due to the relatively small difference in the ionization rates for electrons and holes or because both electrons and holes are injected into the multiplication region. The SAM structure can be used to reduce excess noise factor and also enhance the multiplication noise gain through impact-ionization engineering.[16, 17]

Due to the great band structure engineering flexibility, an antimonide-based SLS can be used as the barrier layer for a multi-quantum well (MQW) heterostructure when combined with an GaSb well. This MQW enables using the antimony-based SLS to engineer a large difference in the ionization rates for electrons and holes by designing the band discontinuities between well and barrier to have a large difference between conduction band offset (ΔE_c) and valence band offset (ΔE_v). As demonstrated by McIntyre[18], a large difference in the ionization rates for electrons and holes is essential for a low noise avalanche photodiode. Therefore, it is promising to use the MQW approach, with antimony-based SLS barriers, as the multiplication layer in the APDs. The separate absorption layer used in the SAM-APD is an InAsSb alloy chosen to cover the mid-infrared range at an operating temperature of 150K.

The MWIR SAM-APD device was grown by molecular beam epitaxy with the multiplication layer consisting of an AlGaAsSb/GaSb MQW. The AlGaAsSb barrier layer in the MQW structure was grown as an $AlAs_{0.1}Sb_{0.9}$/GaSb superlattice, This SLS is called an H-structure superlattice and can be used as an electron barrier layer in some type-II superlattice infrared photodetector designs.[19] For convenience, 'AlGaAsSb' will be used to refer to the AlAsSb/GaSb H-structure superlattice in the rest of discussion. The bandgap energy of the H-structure superlattice was calculated by the empirical tight-binding method (ETBM) to be around 1 eV at 150 K. The effective conduction band of the H-structure superlattice moves upward significantly due to the confinement of the electrons in the GaSb well by the AlAsSb barrier layers. The $InAs_{0.9}Sb_{0.1}$ bulk material was used as the absorption layer for the mid-wavelength infrared detection at 150 K. During the growth, the $InAs_{0.9}Sb_{0.1}$ material in the device structure was grown as InAs-InSb binary-binary digital alloy.[20]

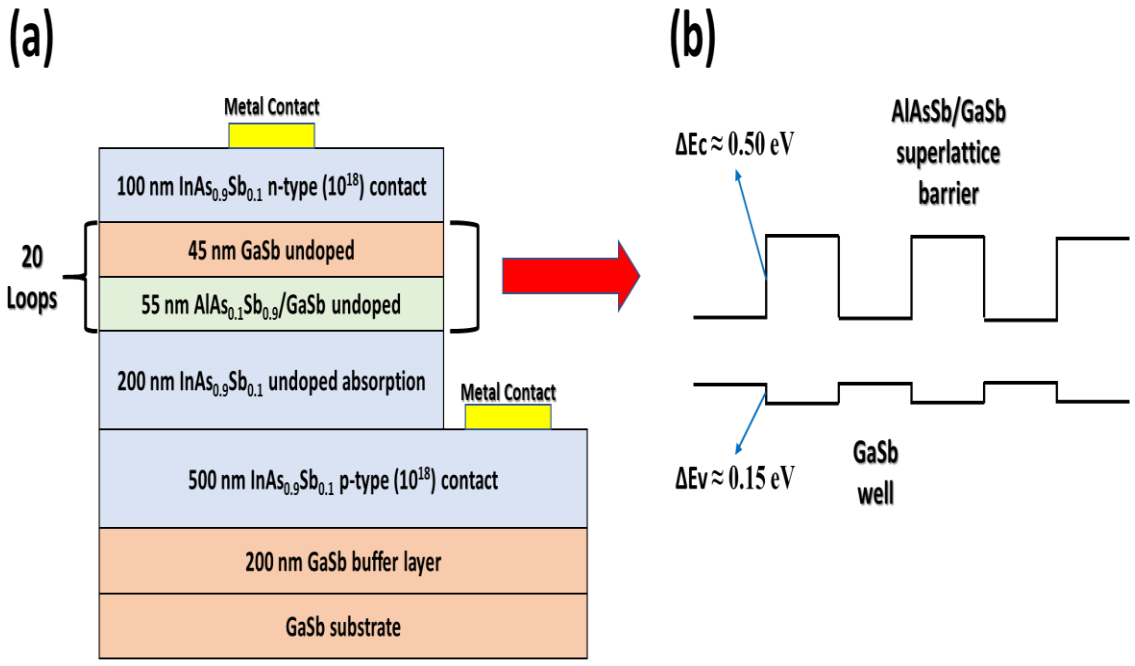

Figure 1. (a) Schematic of the MWIR SAM-APD structure. (b) The band alignment of the MQW consisted of AlAsSb/GaSb superlattice barrier and GaSb well for the multiplication region. The conduction band offset and valence band offset are marked.

The MWIR APD was grown on 2-inch Te-doped n-type (10^{17} cm^{-3}) GaSb (100) substrate using an Intevac Modular Gen II molecular beam epitaxy (MBE) and its device structure is shown in Fig. 1(a). The 200 nm thick GaSb buffer layer and a 500 nm thick p-contact (10^{18} cm^{-3}) $InAs_{0.9}Sb_{0.1}$ layer was grown. A 200 nm undoped $InAs_{0.9}Sb_{0.1}$ absorption layer was grown next. The InAsSb absorption layer was followed by a AlGaAsSb (AlAsSb/GaSb H-structure superlattice) as the barrier layer and GaSb as the well layer. The MQW structure was used as the multiplication layer, as shown in Fig. 1(b). To finish the device, a 100 nm top n-contact (10^{18} cm^{-3}) $InAs_{0.9}Sb_{0.1}$ layer was grown. During growth, silicon and beryllium were used for n-type and p-type dopants, respectively.

The empirical tight-binding method (ETBM) was used to calculate the band discontinuities between the $AlAs_{0.1}Sb_{0.9}$/GaSb superlattice barrier and the GaSb well. The conduction band offset (ΔE_c) and valence band offset (ΔE_v) between the barrier and well in the MQW structure were calculated to be ~0.50 eV and ~0.15 eV, respectively. In this MQW structure, when a hot electron in the AlGaAsSb barrier, accelerated by the applied bias voltage, enters a GaSb well, it abruptly gains energy equal to the conduction band edge (ΔE_c). The net effect is that the electron sees a stronger electric field (increased by ΔE_c) compared to the same conditions in bulk GaSb material. Since the electron impact ionization rate in the GaSb well layer, α'_{GaSb}, increases exponentially with increasing electric field, a large increase in the electron impact ionization rate with respect to bulk GaSb is expected. When the electron enters the next AlGaAsSb barrier, it sees a field decreased by ΔE_c and thus a reduced electron impact ionization rate in the AlGaAsSb barrier layer.[21] However, since $\alpha'_{GaSb} \gg \alpha'_{AlGaAsSb}$, the exponential dependence on the threshold energy ensures that the average electron impact ionization rate $\bar{\alpha}$:[22]

$$\bar{\alpha} = (\alpha'_{GaSb} L_{GaSb} + \alpha'_{AlGaAsSb} L_{AlGaAsSb}) / (L_{GaSb} + L_{AlGaAsSb})$$

is largely increased (L denotes layer thicknesses). In contrast, the hole ionization rate β is not substantially changed by the MQW structure since the valence band discontinuity (ΔE_v) is much smaller. The holes can flow unhindered across the MQW multiplication layer, just the same as the condition in the GaSb bulk material. Therefore, the hole impact ionization rate β in the MQW structure is expected to have a similar value of β as in the bulk GaSb material. In general, the difference between the electron impact ionization rate and the hole impact ionization rate can lead to a large reduction in the β/α ratio and lead to the pure or dominant electron-initiated multiplication mechanism in the MWIR APD.

The grown material was processed into a set of circular photodetectors using conventional photodetector processing.[23] No anti-reflection (AR) coating was applied and the SAM-APD device was kept non-passivated. The test chip was then mounted onto a 68-pin leadless chip carrier (LCC) for electrical and optical characterization. The SAM-APD test chip was loaded into a Janis STVP-100 two chamber liquid helium cryostat station with controlled temperature ranging from 150 K to 200 K.

The relative spectral response of the InAsSb-based MWIR SAM-APD was measured at both 150 K and 200 K under front-side illumination using a Bruker IFS 66v/S Fourier transform infrared spectrometer (FTIR). A calibrated blackbody source at 1000 ℃ was then used to calculate the absolute optical responsivity of the photodiodes.[24] The optical performance of the devices is shown in Figure 2. At 150 K and 200 K, the responsivity for the SAM-APD device reaches a peak value of 2.26 A/W and 3.84 A/W at 4.0 μm under -1.0 V applied bias,

respectively. The device exhibits a 100% cut-off wavelength of ~5.3 µm at 150 K and ~5.6 µm at 200 K.

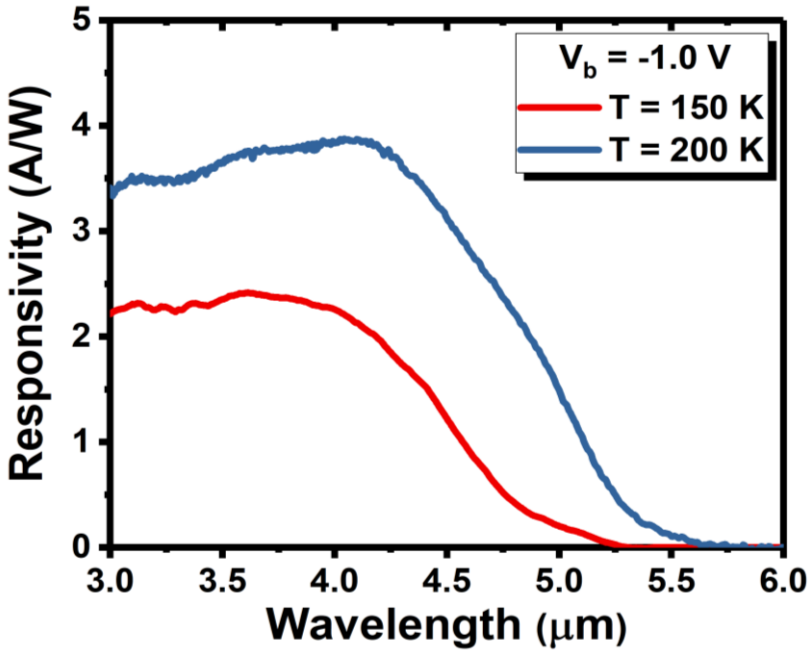

Figure 2. Responsivity spectra of the SAM-APD device under front-side illumination at 150 K (red) and 200 K (blue) under -1.0 V bias voltage.

Current-voltage (I-V) measurements of the SAM-APD sample were carried utilizing an Agilent 4156c semiconductor parameter analyzer. To study the temperature dependent gain characteristics, the measurement temperature for the MWIR InAsSb APDs was varied from 150 to 250 K. A 633 nm He–Ne laser with an incident power of 5.0 mW was used to measure the photocurrent and the gain of the APDs. The multiplication gain was calculated by normalizing the photocurrent, i.e. difference between light and dark currents, by the unity-gain photocurrent.[25] The typical breakdown I-V characteristics of a 200×200 µm^2 MWIR InAsSb APD is shown in Fig. 3. A multiplication gain around 29 was achieved at a reverse bias voltage of −14.7 V at 200 K. As shown in Fig. 4, the gain exhibits an exponential increase as a function of the reverse bias. This demonstrates that the InAsSb-based SAM-APD has the expected exponential multiplication gain characteristic which confirms single carrier electron-dominated impact ionization in the avalanche regime, as seen in other MWIR APDs.[26, 27]

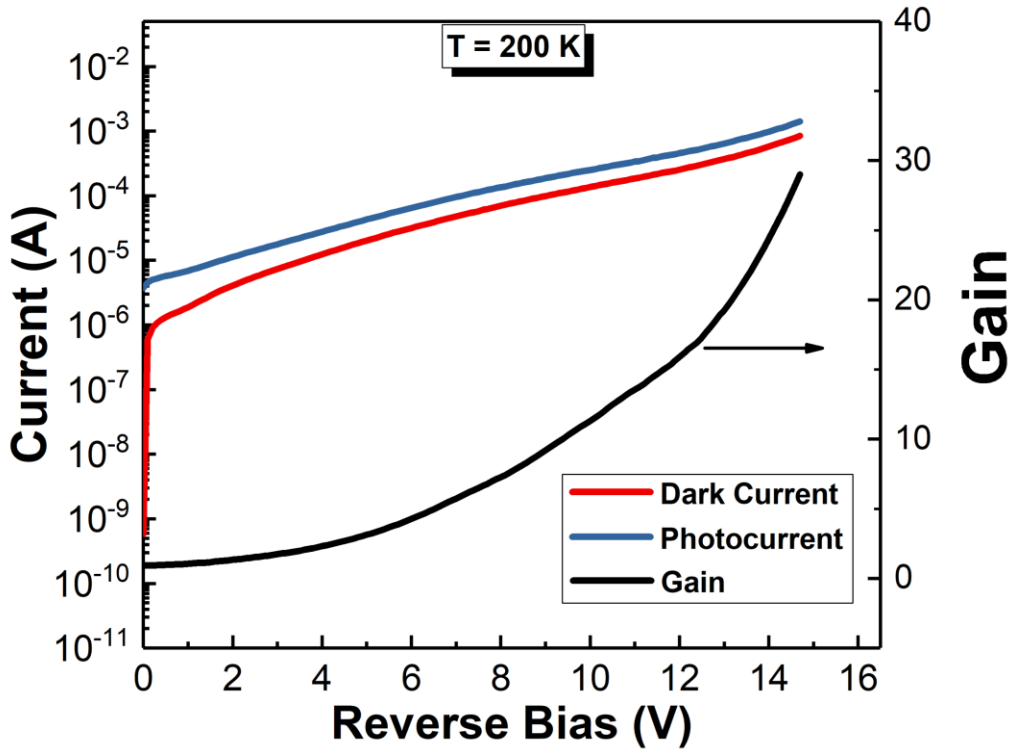

Figure 3. Breakdown I-V characteristics and corresponding multiplication gain vs applied reverse bias at 200 K. Dark current and photocurrent are shown on the left axis; gain is shown on the right axis.

The relationship between the multiplication gain of the SAM-APD device and the temperature was also investigated as shown in Figure 4. The temperature dependent gain characteristic exhibits the trend that the multiplication gain decreases continually from 121 to 10 while the temperature increases from 150 K to 250 K. At 150 K, the maximum multiplication gain, around 121, for the MWIR SAM-APD device was achieved at - 16.8 V bias voltage. The multiplication gain value at 150 K for this device is larger than the previous reports for III-V materials based MWIR APDs.[15] The decrease of the multiplication gain at higher temperature is because the different scattering mechanisms, such as lattice scattering and impurity scattering, become stronger when the temperature increases, making a higher loss of kinetic energy for carriers via scattering. It is more difficult for the carriers to reach the impact ionization threshold energy at higher temperature. In addition, carrier-carrier scattering is an important factor in semiconductor materials where the impact ionization process is significant. The higher probability of carrier-carrier scattering at higher temperature also leads to the decrease of the multiplication gain for the APD device.[28]

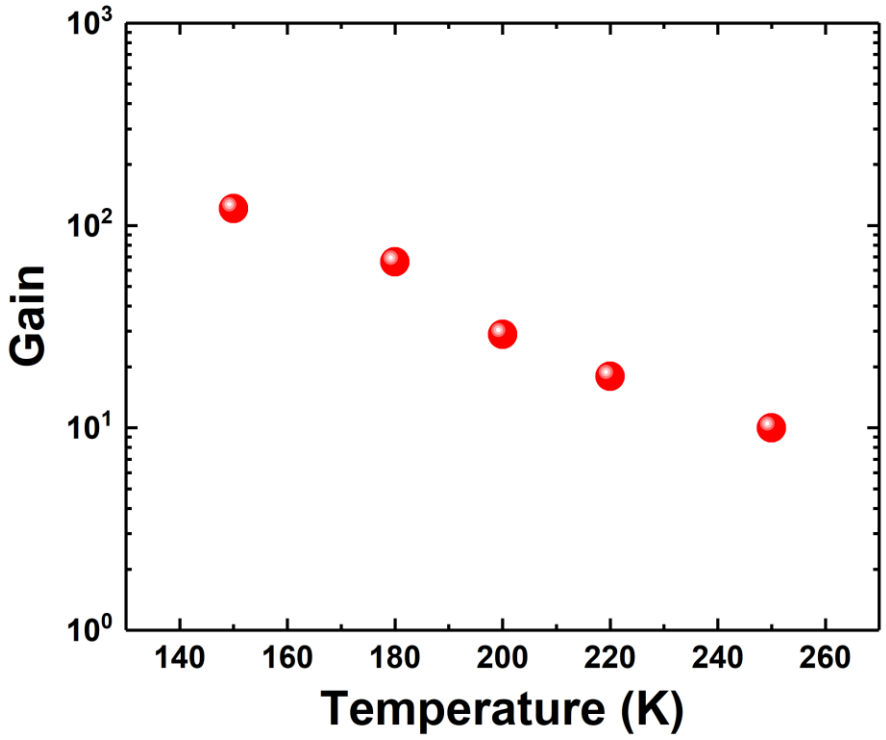

Figure 4: Temperature dependent gain characteristics of the InAsSb-based MWIR SAM-APD.

Another APD device with the flipped structure (the p-type contact at the top and the n-contact at the bottom) was grown and processed under the same conditions to derive the electron and hole impact ionization coefficients, α and β from the experimental value of electron initiated avalanche gain M_e and hole initiated avalanche gain M_h by calculating the following formula,[29]

$$\alpha = \frac{1}{W}\frac{M_e - 1}{M_e - M_h}\ln\frac{M_e}{M_h} \qquad (2)$$

$$\beta = \frac{1}{W}\frac{M_h - 1}{M_h - M_e}\ln\frac{M_h}{M_e} \qquad (3)$$

Where W is the depletion width, i.e., the width of the multiplication layer. Because the multiplication layer is undoped, the electric field is nearly constant across the region. The APD device with the flipped structure was illuminated from top p-type contact, where the carrier injection into the multiplication region is dominated by holes.[30] The derived electron and hole impact ionization coefficients are shown in Fig. 5, where the large difference between α and β is seen. The carrier ionization ratio, *k*, defined as the ratio of hole to electron impact ionization coefficient, for the MWIR SAM-APD was calculated to be ~0.097 at 200 K. This small *k* value is largely due to the enhanced electron impact ionization in MQW multiplication region, which also agrees well with other simulation and experiment results of this effect in similar structures like superlattices in the previous works.[22, 31, 32] The small carrier ionization ratio is essential for achieving low excess noise as demonstrated by McIntyre.[18]

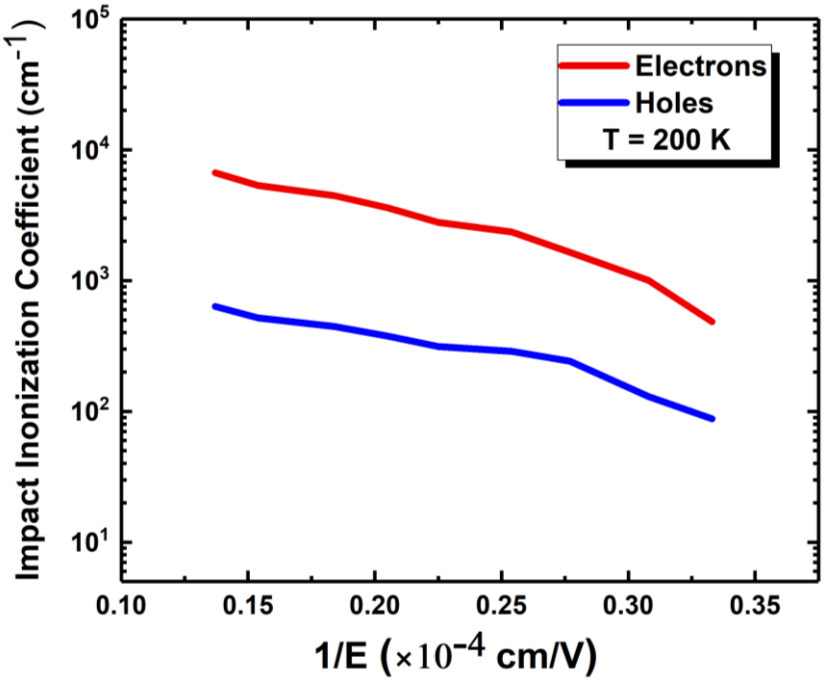

Figure 5: Electron and hole impact ionization coefficients for the MWIR SAM-APD vs inverse of electric field at 200 K.

In summary, the multi-quantum well structure using AlAsSb/GaSb H-structure superlattice was incorporated into an InAsSb-based SAM-APD device as the multiplication region. The SAM-APD device was grown on GaSb substrate by MBE and designed to have electron-dominated avalanche mechanism by engineering the electron impact ionization rate in the MQW structure. The device exhibits a 100 % cut-off wavelength of ~5.3 µm at 150 K and reaches the peak responsivity of 2.26 A/W at 4.0 µm under -1.0 V applied bias. The multiplication gains of 121 and 29 were achieved for the SAM-APD device at 150 K and 200 K, respectively. The carrier ionization ratio was calculated to be 0.097 at 200 K.

Methods

Growth. An Intevac Modular Gen II molecular beam epitaxy (MBE) equipped with group III SUMO cells and group V valved crackers was used to grow the SAM-APD structure on 2-inch Te-doped n-type (10^{17} cm^{-3}) GaSb (100) substrate. During growth, Silicon and Beryllium were used for n-type and p-type dopants, respectively.

Fabrication. After growth, the wafer was fabricated into the two-contact mesa-isolated devices with the sizes varying from 40×40 µm^2 to 300×300 µm^2 using our standard single element photodiode fabrication steps. The photolithography was first used to create the pattern of mesa shapes and sizes on the photoresist above the sample. Then the combination of inductively coupled plasma-reactive ion etching (ICP-RIE) and wet etching was used to transfer the pattern

of the photomask onto the sample to define the shape of the mesa. The wet etching right after ICP-RIE can remove the residue and smoothen the sidewall, which can reduce the surface leakage current. All the devices were cleaned thoroughly during processing to minimize the dark current. A second photolithography was used to define the top and bottom contact areas. Then the top and bottom metal contacts consisted of Ti/Au were deposited via electron beam metal evaporation. A SiO_2 layer was deposited on the sample via plasma enhanced chemical vapor deposition (PECVD) to passivate the devices. The window to the metal contacts was opened by performing another photolithography and removing the SiO_2 by reactive ion etching. The metal contacts for wire-bonding were then deposited.

Device testing. The SAM-APD test chip was mounted onto a 68-pin leadless chip carrier (LCC) and then loaded into a Janis STVP-100 two chamber liquid helium cryostat station with controlled temperature ranging from 150 K to 200 K. The relative spectral response of the InAsSb-based MWIR SAM-APD was measured at both 150 K and 200 K under front-side illumination using a Bruker IFS 66v/S Fourier transform infrared spectrometer (FTIR). A calibrated blackbody source at 1000 ℃ was then used to calculate the absolute optical responsivity of the photodiodes.

Current-voltage (I-V) measurements of the SAM-APD sample were carried utilizing an Agilent 4156c semiconductor parameter analyzer. A 633 nm He–Ne laser with an incident power of 5.0 mW was used to measure the photocurrent and the gain of the APDs at temperature range from 150 K to 250 K.

References

[1] M. Razeghi, *Sb-based third generation at Center for Quantum Devices* (SPIE Defense + Commercial Sensing). SPIE, 2020.

[2] M. Razeghi *et al.*, *Antimonite-based gap-engineered type-II superlattice materials grown by MBE and MOCVD for the third generation of infrared imagers* (SPIE Defense + Commercial Sensing). SPIE, 2019.

[3] J. Li, A. Dehzangi, D. Wu, R. McClintock, and M. Razeghi, "Type-II superlattice-based heterojunction phototransistors for high speed applications," *Infrared Phys Techn,* vol. 108, p. 103350, 2020/08/01/ 2020, doi: https://doi.org/10.1016/j.infrared.2020.103350.

[4] A. Dehzangi, R. McClintock, D. H. Wu, A. Haddadi, R. Chevallier, and M. Razeghi, "Extended short wavelength infrared heterojunction phototransistors based on type II superlattices," (in English), *Appl Phys Lett,* vol. 114, no. 19, May 13 2019. [Online]. Available: <Go to ISI>://WOS:000470152800023.

[5] J. C. Campbell, A. G. Dentai, W. S. Holden, and B. L. Kasper, "High-performance avalanche photodiode with separate absorption 'grading' and multiplication regions," *Electron Lett*, vol. 19, no. 20, pp. 818-820. [Online]. Available: https://digital-library.theiet.org/content/journals/10.1049/el_19830558

[6] L. C. Chuang *et al.*, "GaAs-Based Nanoneedle Light Emitting Diode and Avalanche Photodiode Monolithically Integrated on a Silicon Substrate," *Nano Letters,* vol. 11, no. 2, pp. 385-390, 2011/02/09 2011, doi: 10.1021/nl102988w.

[7] A. Kerlain *et al.*, "Performance of Mid-Wave Infrared HgCdTe e-Avalanche Photodiodes," *Journal of Elec Materi,* vol. 41, no. 10, pp. 2943-2948, 2012/10/01 2012, doi: 10.1007/s11664-012-2087-5.

[8] X. Sun, J. B. Abshire, J. D. Beck, P. Mitra, K. Reiff, and G. Yang, "HgCdTe avalanche photodiode detectors for airborne and spaceborne lidar at infrared wavelengths," *Optics Express,* vol. 25, no. 14, pp. 16589-16602, 2017/07/10 2017, doi: 10.1364/OE.25.016589.

[9] A. Rogalski, "HgCdTe infrared detector material: history, status and outlook," *Reports on Progress in Physics,* vol. 68, no. 10, p. 2267, 2005. [Online]. Available: http://stacks.iop.org/0034-4885/68/i=10/a=R01.

[10] P. Castelein *et al.*, *Megapixel HgCdTe MWIR focal plane array with a 15-um pitch* (AeroSense 2003). SPIE, 2003.

[11] B.-M. Nguyen, "Theoretical Design and Material Growth of Type-II Antimonide-based Superlattices for Infrared Detection and Imaging," 01/01 2010.

[12] M. Razeghi, "9 - InAs/GaSb type II superlattices: A developing material system for third generation of IR imaging," in *Mid-infrared Optoelectronics*, E. Tournié and L. Cerutti Eds.: Woodhead Publishing, 2020, pp. 379-413.

[13] A. Haddadi, A. Dehzangi, S. Adhikary, R. Chevallier, and M. Razeghi, "Background–limited long wavelength infrared InAs/InAs1− xSbx type-II superlattice-based photodetectors operating at 110 K," *APL Materials,* vol. 5, no. 3, p. 035502, 2017, doi: 10.1063/1.4975619.

[14] J. Li, A. Dehzangi, D. Wu, R. McClintock, and M. Razeghi, "Resonant cavity enhanced heterojunction phototransistors based on Type-II superlattices," *Infrared Phys Techn,* p. 103552, 2020/10/27/ 2020, doi: https://doi.org/10.1016/j.infrared.2020.103552.

[15] A. Dehzangi, J. Li, L. Gautam, and M. Razeghi, "Avalanche Photodetector Based on InAs/InSb Superlattice," *Quantum Reports,* vol. 2, no. 4, pp. 591-599, 2020.

[16] J. C. Carrano *et al.*, "GaN avalanche photodiodes," *Appl Phys Lett,* vol. 76, no. 7, pp. 924-926, 2000, doi: 10.1063/1.125631.

[17] J. L. Pau, C. Bayram, R. McClintock, M. Razeghi, and D. Silversmith, "Back-illuminated separate absorption and multiplication GaN avalanche photodiodes," *Appl Phys Lett,* vol. 92, no. 10, p. 101120, 2008/03/10 2008, doi: 10.1063/1.2897039.

[18] R. J. McIntyre, "Multiplication noise in uniform avalanche diodes," *IEEE Transactions on Electron Devices,* vol. ED-13, no. 1, pp. 164-168, 1966, doi: 10.1109/T-ED.1966.15651.

[19] A. Haddadi, R. Chevallier, A. Dehzangi, and M. Razeghi, "Extended short-wavelength infrared nBn photodetectors based on type-II InAs/AlSb/GaSb superlattices with an AlAsSb/GaSb superlattice barrier," *Appl Phys Lett,* vol. 110, no. 10, p. 101104, 2017, doi: 10.1063/1.4978378.

[20] T. Schuler-Sandy *et al.*, "Growth of InAs–InAsSb SLS through the use of digital alloys," *J Cryst Growth,* vol. 425, pp. 29-32, 2015/09/01/ 2015, doi: https://doi.org/10.1016/j.jcrysgro.2015.02.096.

[21] M. Ren, S. Maddox, Y. Chen, M. Woodson, J. C. Campbell, and S. Bank, "AlInAsSb/GaSb staircase avalanche photodiode," *Appl Phys Lett,* vol. 108, no. 8, p. 081101, 2016, doi: 10.1063/1.4942370.

[22] F. Capasso, W. T. Tsang, A. L. Hutchinson, and G. F. Williams, "Enhancement of electron impact ionization in a superlattice: A new avalanche photodiode with a large ionization rate ratio," *Appl Phys Lett,* vol. 40, no. 1, pp. 38-40, 1982, doi: 10.1063/1.92910.

[23] D. Wu, J. Li, A. Dehzangi, and M. Razeghi, "Mid-wavelength infrared high operating temperature pBn photodetectors based on type-II InAs/InAsSb superlattice," *AIP Advances,* vol. 10, no. 2, p. 025018, 2020, doi: 10.1063/1.5136501.

[24] J. Li, A. Dehzangi, D. Wu, and M. Razeghi, *High speed short wavelength infrared heterojunction phototransistors based on type II superlattices* (SPIE OPTO). SPIE, 2020.

[25] C. Bayram, J. L. Pau, R. McClintock, M. Razeghi, M. P. Ulmer, and D. Silversmith, "High quantum efficiency back-illuminated GaN avalanche photodiodes," *Appl Phys Lett,* vol. 93, no. 21, p. 211107, 2008, doi: 10.1063/1.3039061.
[26] S. Mallick *et al.*, "Ultralow noise midwave infrared InAs–GaSb strain layer superlattice avalanche photodiode," *Applied Physics Letters,* vol. 91, no. 24, p. 241111, 2007.
[27] M. Kinch, J. Beck, C.-F. Wan, F. Ma, and J. Campbell, "HgCdTe electron avalanche photodiodes," *Journal of Elec Materi,* vol. 33, no. 6, pp. 630-639, 2004.
[28] R. Binder, D. Scott, A. E. Paul, M. Lindberg, K. Henneberger, and S. W. Koch, "Carrier-carrier scattering and optical dephasing in highly excited semiconductors," *Physical Review B,* vol. 45, no. 3, pp. 1107-1115, 01/15/ 1992, doi: 10.1103/PhysRevB.45.1107.
[29] C. A. Lee, J. J. Kleimack, R. L. Batdorf, W. Wiegmann, and R. A. Logan, "Ionization Rates of Holes + Electrons in Silicon," (in English), *Physical Review,* vol. 134, no. 3a, pp. A761-+, 1964, doi: DOI 10.1103/PhysRev.134.A761.
[30] I. H. Oguzman, E. Bellotti, K. F. Brennan, J. Kolnik, R. P. Wang, and P. P. Ruden, "Theory of hole initiated impact ionization in bulk zincblende and wurtzite GaN," (in English), *Journal of Applied Physics,* vol. 81, no. 12, pp. 7827-7834, Jun 15 1997, doi: Doi 10.1063/1.365392.
[31] K. Brennan, "Theory of electron and hole impact ionization in quantum well and staircase superlattice avalanche photodiode structures," *IEEE Transactions on Electron Devices,* vol. 32, no. 11, pp. 2197-2205, 1985, doi: 10.1109/T-ED.1985.22258.
[32] P. Aristin, A. Torabi, A. K. Garrison, H. M. Harris, and C. J. Summers, "New doped multiple‐quantum‐well avalanche photodiode: The doped barrier Al0.35Ga0.65As/GaAs multiple‐quantum‐well avalanche photodiode," *Appl Phys Lett,* vol. 60, no. 1, pp. 85-87, 1992, doi: 10.1063/1.107383.

Acknowledgments

This work was partially supported by the Defense Advanced Research Projects Agency (DARPA) under agreement number FA8650- 18-1-7810. Authors would like to acknowledge the support and encouragement of Dr. Whitney Mason from DARPA., support and encouragement of Dr. Michael Gerhold and Dr. Tania Paskova from the U.S. Army Futures Command, Dr. Kurt Eyink from the Air Force Research Laboratory, Dr. Murzy Jhabvala from NASA Goddard Space Flight Center, and Dr. Meimei Tidrow from the U.S. Army Night Vision, Laboratory.

Figures

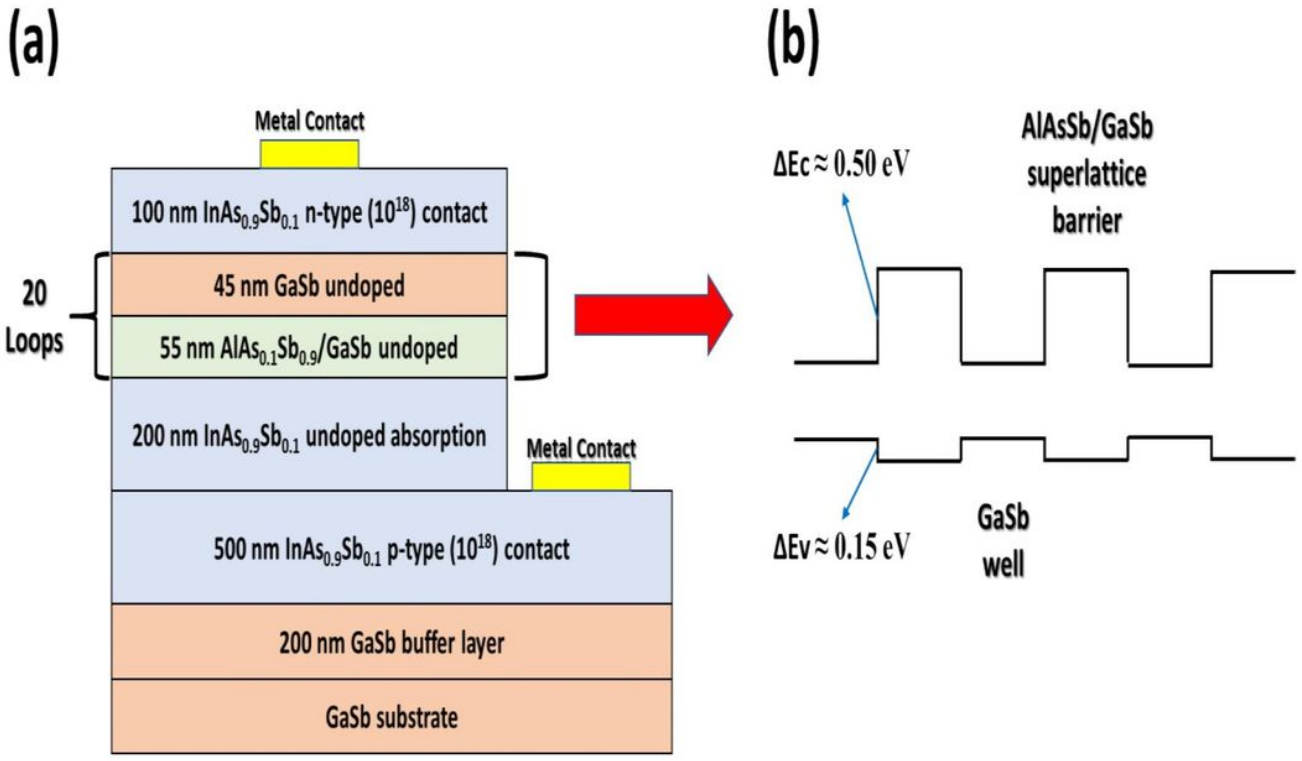

Figure 1

(a) Schematic of the MWIR SAM-APD structure. (b) The band alignment of the MQW consisted of AlAsSb/GaSb superlattice barrier and GaSb well for the multiplication region. The conduction band offset and valence band offset are marked.

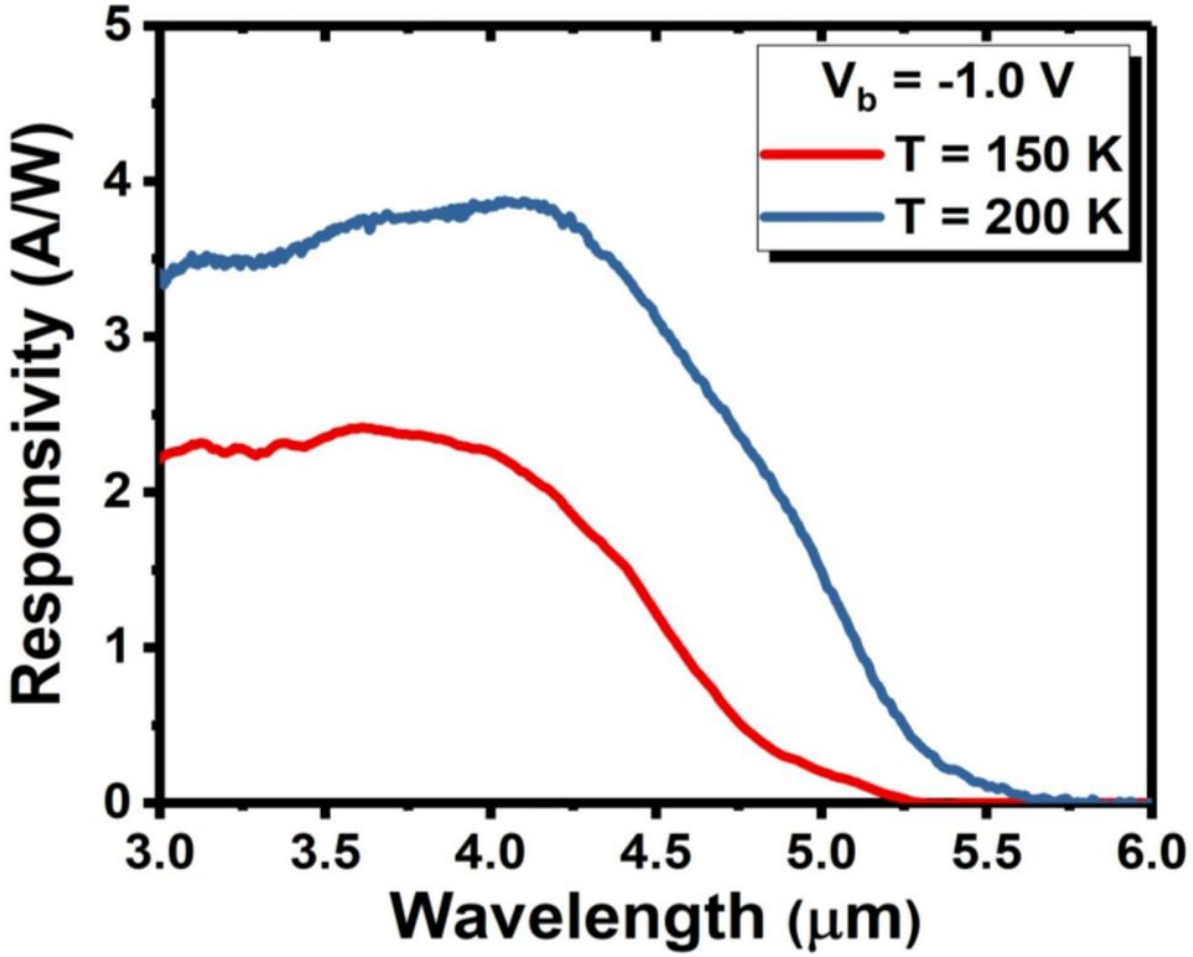

Figure 2

Responsivity spectra of the SAM-APD device under front-side illumination at 150 K (red) and 200 K (blue) under -1.0 V bias voltage.

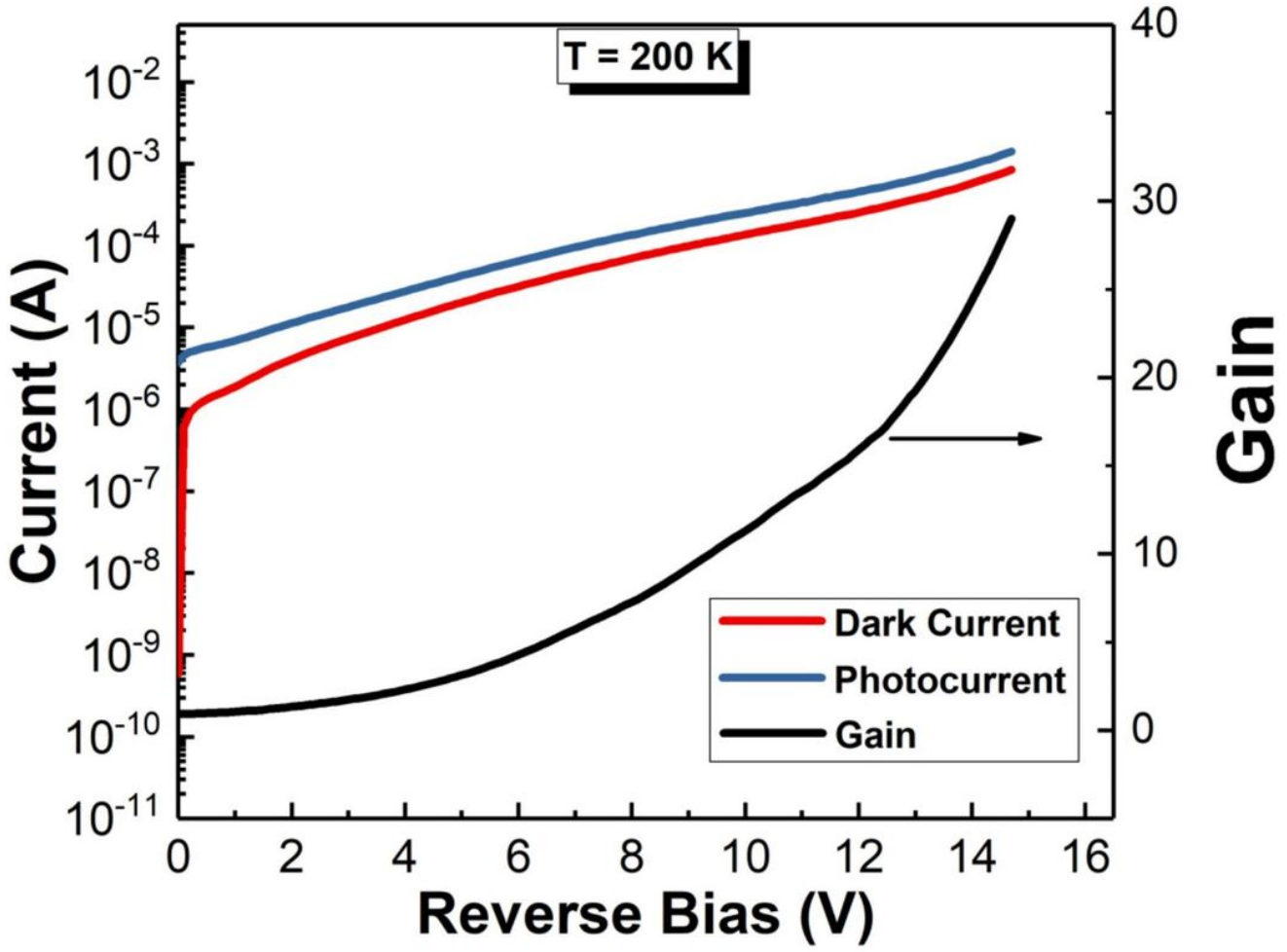

Figure 3

Breakdown I-V characteristics and corresponding multiplication gain vs applied reverse bias at 200 K. Dark current and photocurrent are shown on the left axis; gain is shown on the right axis.

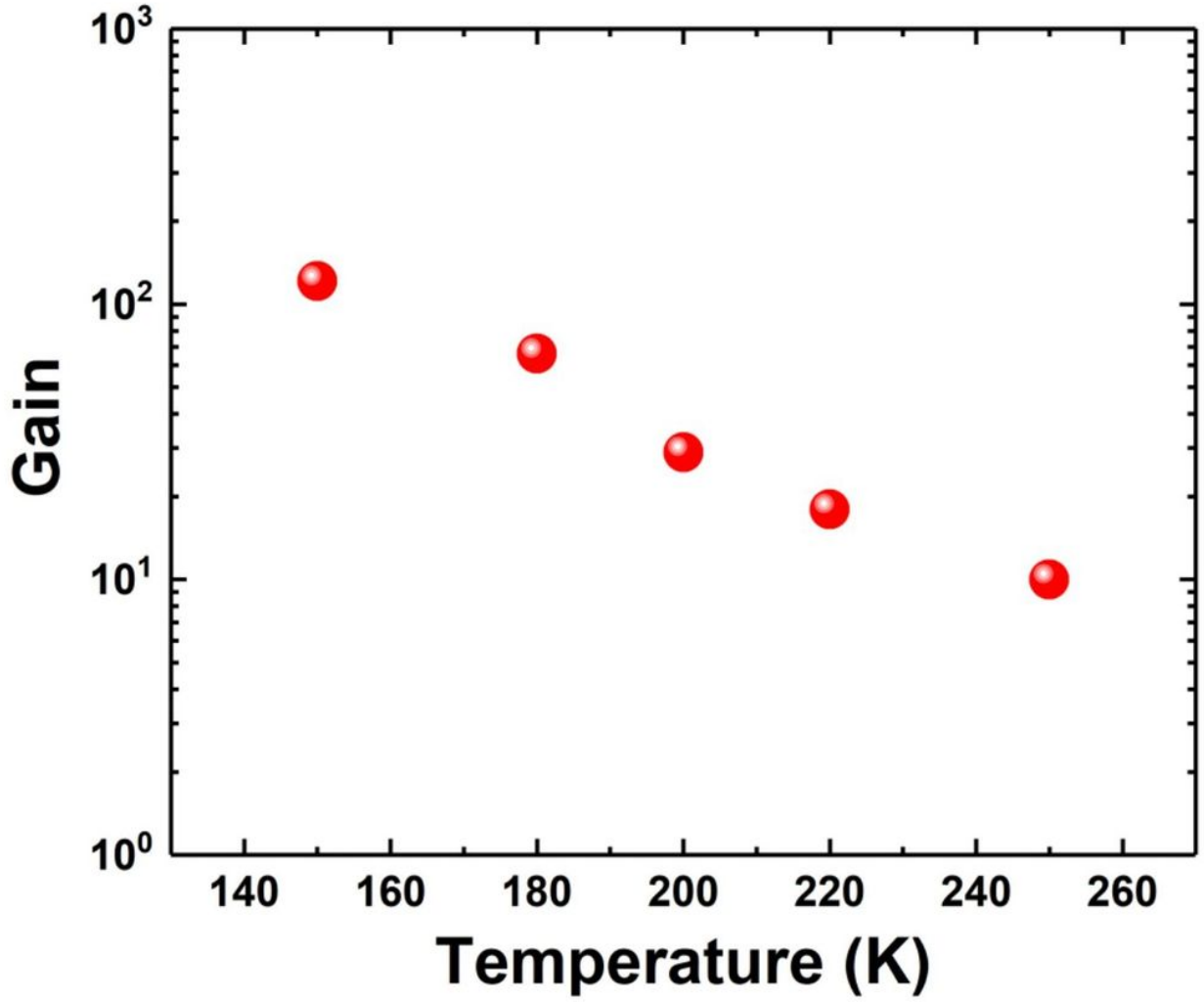

Figure 4

Temperature dependent gain characteristics of the InAsSb-based MWIR SAM-APD.

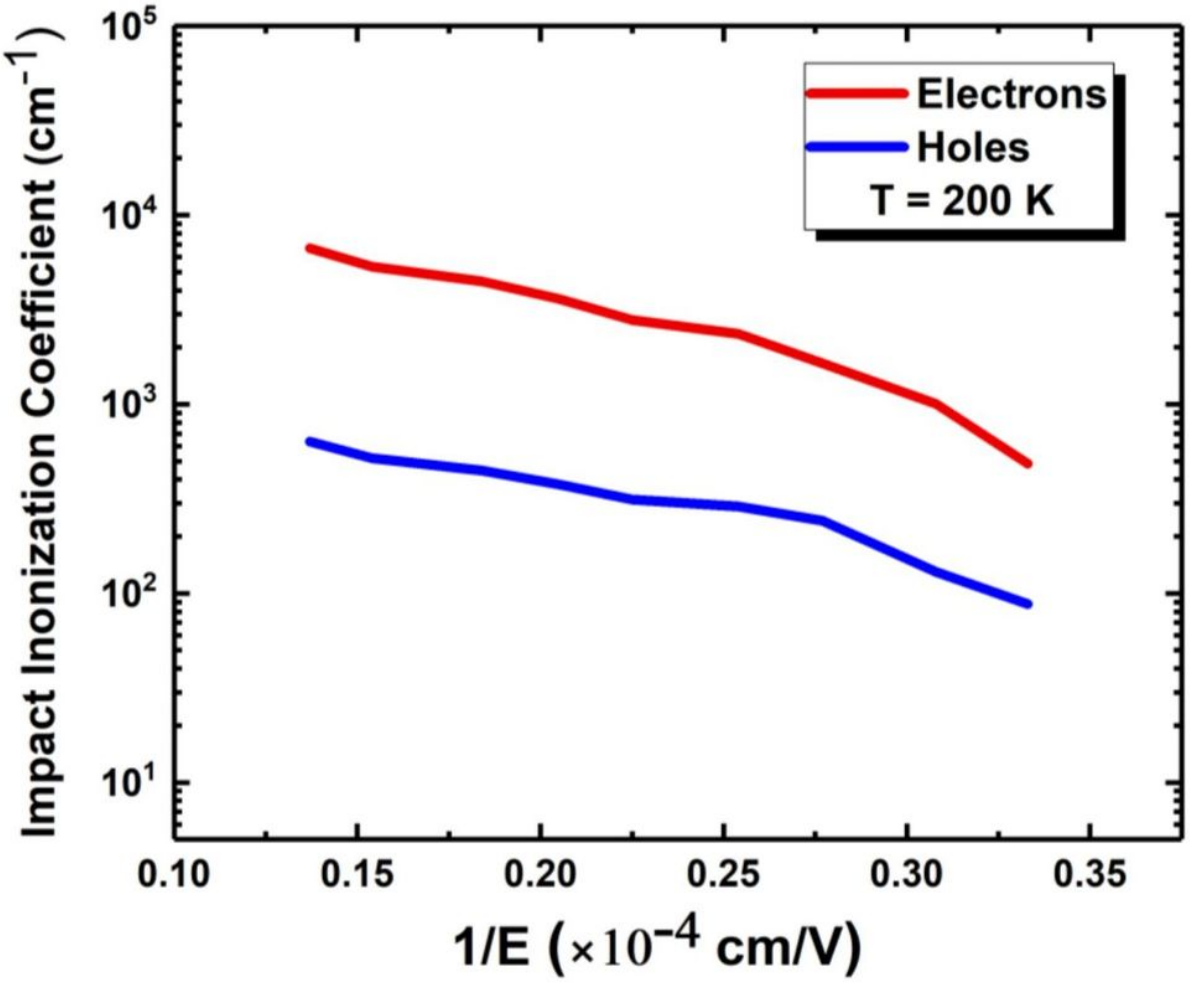

Figure 5

Electron and hole impact ionization coefficients for the MWIR SAM-APD vs inverse of electric field at 200 K.